We are IntechOpen, the world's leading publisher of Open Access books Built by scientists, for scientists

6,900
Open access books available

186,000
International authors and editors

200M
Downloads

Our authors are among the

154
Countries delivered to

TOP 1%
most cited scientists

12.2%
Contributors from top 500 universities

WEB OF SCIENCE™

Selection of our books indexed in the Book Citation Index in Web of Science™ Core Collection (BKCI)

Interested in publishing with us?
Contact book.department@intechopen.com

Numbers displayed above are based on latest data collected.
For more information visit www.intechopen.com

Chapter

Interfacial Phenomena in the Synthesis Process of Barium Sulfate Particles Precipitated in a Lobed Inner Cylinder Taylor-Couette Flow Reactor: Effects of Fluid Dynamics

Lu Liu, Guang Li, Xiaogang Yang, Xiani Huang and Chenyang Xue

Abstract

Three different kinds of morphology with various sizes of barium sulfate particles were produced by reactive precipitation in a Taylor-Couette flow reactor. It is found that particle morphology transition is strongly related to the hydrodynamics in the reactor, clearly indicating an interfacial interaction between feed solutions and aggregated particles. At low concentration, particle morphology transition is observed at the onset of turbulent Taylor-Couette flow. Such morphology transition also appears at the onset of turbulent Taylor vortex flow at high concentration. Based on different transition status, supersaturation is found to play an important role in nucleation and growth processes. In addition, it is revealed that the synthesized particle reduces its size as the consequence of the transition in particle morphology, indicating the effect of variation of the feeding rates. Experimental results have confirmed that controllable synthesis of barium sulfate particles with a particular morphology can be achieved through suitable selection of the controlling parameters such as the rotational speed of inner cylinder of Taylor-Couette flow reactor, reactant feeding rate and supersaturation ratio.

Keywords: barium sulfate, Taylor-Couette reactor, particle morphology, flow pattern, supersaturation, agglomeration

1. Introduction

Precipitation is a traditional industrial process to produce solid particles. It has been used in many applications. Typical examples can be found in fabrication of pigments, ceramics, pharmaceuticals and bio-chemicals among others. For various purposes, the requirements of particle property are different. As particle size and morphology play important roles in determining particle property [1], many previous studies have paid attention to realization of particle size distribution control and

IntechOpen

to acquirement of a particular morphology [2–4]. As many factors can affect final particle property, such as reactant concentration, feeding modes, additives, and reactor system, their interrelationships are complicated so that many precipitation mechanisms have been proposed [5]. However, none of these proposed precipitation mechanisms can fully address the dynamic processes involved for synthesis of the particles given a particular reactor system. The present work focuses on the effects of three main parameters, rotational speed, feeding rate and supersaturation when employing a Taylor-Couette reactor for synthesis of particles on the change of particle morphology, in particular investigating barium sulfate system. Even though the synthesis of barium sulfate particles has been extensively studied [6–8], controllable synthesis of the particles is still not fully understood, which requires further investigations.

Barium sulfate is a sparingly soluble salt, whose crystallization kinetics has been widely studied. Also, its precipitation system from aqueous barium chloride and sodium sulfate is available according to a series of studies by Nielsen [9–11]. In terms of particle morphology, a number of studies have been conducted to investigate different aspects of the potential possible factors. Many morphologies were observed in connection with the synthesis processes, involving tabular particles (or flat particles), dendritic particles, round-shaped particles (or spherical particles), rhombic particles and rice-shaped particles. Barresi et al. [12] produced barium sulfate particles in a continuous Couette reactor, and they observed dendritic tabular crystals and tabular crystals with pyramidal by changing supersaturation, rotational speed and internal diameter of inner cylinder at the same time. They suggested that supersaturation was the dominant factor in determining particle morphology and size. However, they failed to reveal the effect of each individual variable. Marchisio et al. [13] found a series of morphology change from tabular particles, then dendritic particles to rounded-shaped particles with increase of sodium sulfate concentration. They indicated that the excess of species had a stronger effect on particle morphology due to the preferential absorption of the excess ion. The effect of additives, such as EDTA, phosphate, and lanthanum, has been widely investigated experimentally in their study. From the results as reported by Li et al. [14], various morphologies of barium sulfate particles were exhibited when treatment is done by using polyacrylic acid, such as ellipsoids, monodisperse spheres and rose-like aggregates. They contributed the occurrence of these morphologies to the interactions between carboxyl groups of the additive and inorganic ions. However, the mechanism of randomly coiled conformation of the additive was not clearly illustrated, which results in controllable preparation of each morphology in industrial application to be still questionable. By means of barium sulfate precipitation system, Baldyga and his co-workers [15–17] have experimentally conducted a number of studies using the mixing tank and numerically explored the mixing behavior, aiming at fundamentally reveal the mechanism involved. During this process, they found that various parameters, including feed volume ratio, stirred speed, feeding time, volume ratio, initial concentration and stoichiometric ratio have impacts on particle size distribution and morphology. Also, they proposed a mixing-precipitation model which reasonably described the interaction between the micro-mixing timescale and reaction timescale, consistent with the experimental results. Pagliolico et al. [18] have also illustrated the effect of the mixing on the production of various morphologies of barium sulfate, including dendritic particles, tabular particles, rose aggregates. They proposed shape factors for qualitative description of different morphologies. It can be seen that the abovementioned studies have focused on the effect of both solution conditions (typically excessive species, additives or supersaturation) and operating parameters (typically stirred speed, feeding point location, or addition time) on particle properties. However,

most of deductions in these studies only focused on the change of particle size with the parameters as mentioned while the obtained results just showed the morphology for a particular condition. Little attention has been paid on how the morphology transits with respect to the variations of operating parameters and the correlations between the morphology and these parameters, in particular flow field environment and initial solution conditions.

Taylor-Couette reactors have been employed to prepare different kinds of particles due to its advantages [3, 6, 19]. As no stirrer is involved, the breakage of particles due to the elastic collision can be avoided. Taylor-Couette flow reactor consists of two co-axial cylinders, whose internal cylinder is rotating while the external cylinder is usually kept stationary. The typical characteristics of hydrodynamics of the reactor are a narrow shear rate distribution and relatively uniform kinetic energy dissipation. An increase in the rotational speed can effectively enhance the mixing efficiency. Jung et al. [3] employed a Taylor-Couette reactor to prepare calcium carbonate particles in a gas–liquid system. After comparing the effects of species excess and shear stress, they suggested that the excessive species have a stronger effect on synthesized particle size and morphology while the effect of flow dynamics on the synthesis can be negligible. It should be pointed out, however, that their analysis focused on the aspect of mass transfer, and overlooked the effect of shear rate variations. Mayra and Kim [20] and Thai et al. [19] have systematically conducted a series of studies on the synthesis of Ni-rich hydroxide crystals, a kind of cathode material for lithium ion battery, by using the Taylor-Couette crystallizer. They have clearly demonstrated that under the condition that the Taylor-Couette reactor operates in the range of the critical Reynolds number based on different gap sizes (Re_c = 128.5–219.4), the formed Taylor vortices promote the mixing and enhance the mixing residual time, which yields the uniform agglomerate particles with high tap density. This clearly indicates that the hydrodynamics of the Taylor-Couette flow reactor will have a significant impact on the synthesis of particles and the particle crystals growth.

Even though reactive precipitation processes are very fast, Barresi et al. [12] have demonstrated that mixing, especially micro-mixing, has a significant influence on the precipitation process itself. The mixing in mixing vessels that is caused by shear can be characterized by macro-mixing, meso-mixing, and micro-mixing. According to engulfment-deformation-diffusion model (EDD) as proposed by Baldyga and Bourne [21], engulfment due to the micro-mixing generates the local supersaturation and dilution of species. Such local supersaturation is the driving force for crystallization. Macro-mixing occurs on the scale of the reactor, functioning to convey the reactive solutions throughout the entire available space of the reactor [22]. Macro-mixing provides the environment for the following mixing processes, and affects the distribution of supersaturation. Meso-mixing refers to the exchange of fresh feed and its surroundings on a coarse scale, lager than Kolmogorov scale, but smaller than integral scale of turbulence. It can influence micro-mixing by changing the local environment [23]. Micro-mixing brings the fluid elements into contact, followed by molecular diffusion. It controls the generation of supersaturation.

The aim of the present study is to investigate the morphology transition process of barium sulfate precipitated in a Taylor-Couette reactor with a lobed internal cylinder [24]. The effects of three parameters, rotational speed, feeding rate, and supersaturation, on the synthesized particle morphology are assessed and the correlations are obtained. In order to examine the effect of hydrodynamics characterized by shear rate which closely associates with the rotational speed, a wide range of rotational speeds were chosen varying from 25 to 1000 rpm. The interrelationship of shear rate and final particle morphology is acquired. Then, results will be discussed from the perspective of micro-mixing, as precipitation process is

triggered by supersaturation, whereas micro-mixing controls the generation of local supersaturation. The experimental data obtained from current work can be used for the further validation of multiphase micro-mixing model.

2. Wettability and interfacial phenomena—implications for barium sulfate particle precipitated using a lobed inner cylinder Taylor-Couette flow reactor

The role of surface phenomena and contacts can play significant roles in the transitions of particle morphologies during precipitation. From the preceding section, it can be seen that the formation of different types of particles is related to interfacial phenomenon between liquid and particles. The effects of fluid behavior on particles are embodied mainly from two aspects. On one hand, fluid flow in the reactor contributes to the interfacial ion concentration distribution, thus affecting the mass transfer to the aggregated crystal nuclei for formation of barium sulfate particles. Concentration gradient between nuclei surface (so referred to as equilibrium concentration) and bulk solution (so called bulk concentration) is the driving force for particle growth. During this process, in spite of molecular diffusion, convection dispersion resulted from fluid flow has a dominant effects. Many previous studies (e.g., [25–27]) have adopted Sherwood number, defined as the ratio of convective mass transfer to diffusive mass transport, to characterize the mass transfer contributed from turbulence on fluid-particle interface for particle size ranging from macro-particles to micro-particles. This contribution comes from eddy fluctuation, thus indicating that the shear caused by turbulent eddies may play an important role in the formation of particles in the precipitation. Armenante and Kiwan [28] proposed the correlation with Sherwood number for estimation of the mass transfer coefficient for description of the dissolution process of AgCl crystal. They have reaffirmed the effect of turbulence by applying different power input to the mixing tank reactor, and obtained an improved correlation between the Sherwood number and Reynolds number. Furthermore, Jung et al. [3] have obtained different calcium carbonate morphologies by changing the wall shear stress of the Taylor-Couette flow reactor used in their study. They interpreted this phenomenon from the point of view that ion adsorption takes place on the particle surface while the concentration gradient of adsorbed ions is also caused by shear stress. Thus, interfacial turbulence induced shear has an impact on aggregation. Bubakova et al. [29] proposed an equation to describe the relationship between aggregate size and average shear rate of turbulent eddies formed in the mixing process. Similarly, for the process of Ni-rich hydroxide preparation, Mayra and Kim [20] have also confirmed the parameters that are strongly associated with the fluid shear can have significant influence on agglomeration process. They have indicated that individual crystals can stack together to form irregular aggregates with fluid flow (mainly characterized by turbulent eddy motion), and then shear force generated by turbulent eddies can facilitate these aggregates to bind together to form regular agglomerates. Thus, it may be concluded that interfacial ion concentration and interfacial fluid shear between the solution and particles have significant influences on particle growth and aggregation.

3. Theoretical modeling

3.1 Precipitation process dynamical model

The chemical reaction between aqueous solutions of barium chloride and sodium sulfate obeys the following equation,

$$BaCl_{2(aq)} + Na_2SO_{4(aq)} \rightarrow BaSO_{4(s)} + 2NaCl_{(aq)} \tag{1}$$

The precipitation process of barium sulfate involves four main steps, nucleation, growth, agglomeration and breakup. The driving force of nucleation is supersaturation, which has effects on subsequent processes. Supersaturation σ is defined as the ratio of molar chemical potential φ (the molar Gibbs free energy) in supersaturated solution to the potential in saturated solution [23], being expressed by the activities of ions, a,

$$\sigma = \frac{\varphi - \varphi_{eq}}{RT} = ln\frac{a}{a_{eq}} \tag{2}$$

where a_{eq} is the activity in equilibrium, R is gas constant, and T is absolute temperature. The relationship between ion activity and concentration can also be described as follows:

$$a = \gamma_{\pm} c \tag{3}$$

where $\gamma_{\pm}$ is the activity coefficient. Estimation of $\gamma_{\pm}$ has been proposed by Debye and Huckel [30], and the modified equation is usually adopted, given by

$$lg\gamma_{\pm} = -0.511 z_{+} z_{-} \left(\frac{\sqrt{I}}{1 + \sqrt{I}} - 0.2\sqrt{I} \right) \tag{4}$$

where z is the charge number, and I is the ionic strength, calculated by the following equation

$$I = \frac{1}{2} \sum_{i=1}^{n} c_i z_i^2 \tag{5}$$

where c_i is the molar concentration of species i. Since supersaturation is often expressed as the concentration difference Δc with saturation ratio S defined as the ratio of dissolved concentration to the equilibrium solubility and Sa as a relative saturation ratio, then

$$\Delta c = a - a_{eq} \tag{6}$$

$$S = \frac{a}{a_{eq}} = \sqrt{\frac{a_{Ba^{2+}} a_{SO_4^{2-}}}{K_{SP}}} \tag{7}$$

$$S_a = S - 1 \tag{8}$$

where K_{sp} is the solubility product of barium and sulfate ions in the equilibrium state ($\sim 1.1 \times 10^{-10}$ mol^2/L^2 at 20°C). In the present work, we used S to describe the supersaturation of the system for the following calculation.

During precipitation, new particles are created by nucleation. Molecules of the reactants are combined to generate embryos when the energy required excesses energy barrier ΔG. During this process, there is an induction period which is the necessary time to form a characteristic, significant number of nuclei. This time can also be regarded as the time elapsed from the mixing of reactants to the appearance of nuclei [31], an empirical expression for barium sulfate reaction [32] can be used to estimate t_N

$$lgt_N = 15.5 lg^{-2} S - 4.2 \tag{9}$$

Nucleation rate can be described using the following equation

$$J = k_N \Delta c^n \tag{10}$$

where n is the kinetic order of nucleation. In barium sulfate system, for $\Delta c < 0.01$ mol/L, $k_N = 6 \times 10^{14}$, $n = 1.775$; for $\Delta c > 0.01$ mol/L, $k_N = 2.53 \times 10^{39}$, $n = 15$ [15].

Once nuclei have been formed, they start to grow to a particular shape and size. This process can be integrated into two steps: the mass transfer to the solid–solution interface, and the surface integration of growth units diffused into the crystal lattice. The total growth rate given by

$$B = k_g (S-1)^2 \tag{11}$$

where k_g is growth coefficient. At a temperature of 20°C, $k_g = 4 \times 10^{-11}$ m/s.

3.2 Taylor-Couette vortex flow

Flow pattern in a Taylor-Couette flow reactor can be characterized using the Reynolds number, defined by

$$\mathrm{Re} = \frac{\omega_i r_i \delta_{eq}}{\nu} \tag{12}$$

where ω_i is the rotational speed of the inner cylinder, r_i is the equivalent radius of inner cylinder, estimated based on the ratio of four times of the inner cylinder cross-section area to the wetted perimeter of the cylinder, δ_{eq} is the equivalent gap between the inner cylinder and outer cylinder and ν is the kinematic viscosity of suspension, the ratio of the dynamic viscosity to the density of the fluid. The dynamic viscosity can be measured using a viscometer. For a fixed outer cylinder, with the increase of the rotational speed of inner cylinder exceeding a critical Reynolds number, the circular Couette flow becomes unstable, and Taylor vortices appear in pairs. Taylor vortex flow is a kind of secondary flow, superimposed on the laminar Couette flow. The velocity profiles of Couette flow and Taylor vortex are shown in **Figure 1** respectively. Radial and axial velocities manifest once Taylor vortices appear.

At low rotational speed, the driven flow can be considered as laminar Couette flow, and the fluid velocity is mainly determined by azimuthal velocity, as the highest radial and axial velocities are less than 15% of azimuthal velocity [33]. The azimuthal velocity profile in the gap for incompressible fluid takes the form of

$$u_\theta = Ar + \frac{B}{r} \tag{13}$$

where u_θ is the azimuthal velocity. A and B depend on the radius ratio $\eta = r_i/r_o$ and the cylinder angular velocity ratio $\zeta = \omega_o/\omega_i$.

$$A = \omega_i \frac{\zeta - \eta^2}{1-\eta^2}, B = \omega_i \frac{r_i^2(1-\zeta)}{1-\eta^2} \tag{14}$$

Then, further increase in rotational speed leads to series of instabilities occurs, changing from laminar flow including Taylor vortex flow, wavy Taylor vortex flow, modulated wavy Taylor vortex flow, to turbulent flow including turbulent Taylor

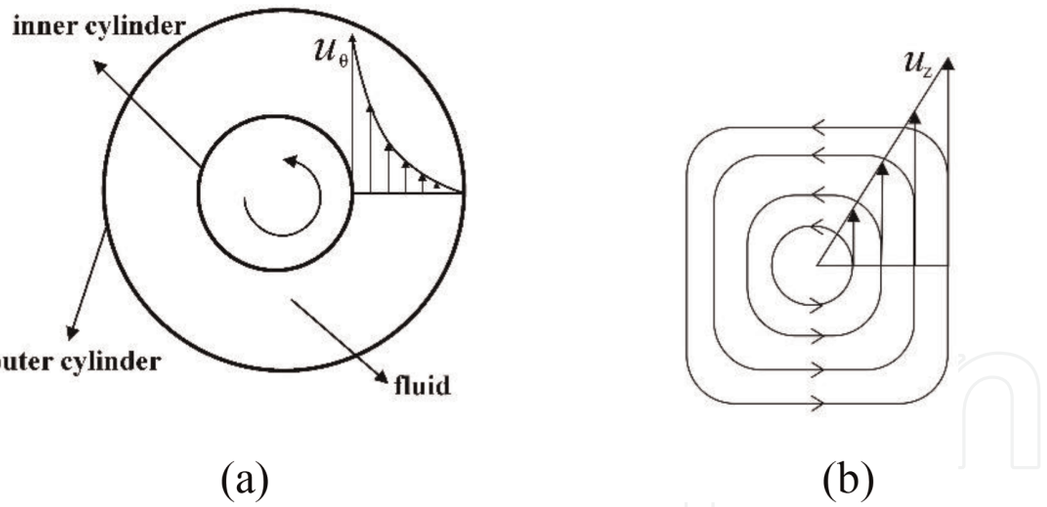

Figure 1.
(a) Azimuthal velocity profiles of circular Couette flow, and (b) axial velocity of Taylor vortex.

vortex flow and fully developed turbulent Taylor flow. These flow patterns are influenced by the use of different aspect ratio and radius ratio. DiPrima et al. [34] have summarized the effects of a series of radius ratio on the flow patterns and some previous studies have investigated the transition points of these patterns [35–37]. At high rotational speed, radial and axial velocities cannot be ignored due to the enhanced effect of Taylor vortices. The mean velocity can be approximately estimated by.

$$\overline{u} = \frac{2\omega_i r_i^2}{3\left(r_o^2 - r_i^2\right)}\left(r_i^3 + 2r_o^3 - 3r_i r_o^2\right) \tag{15}$$

4. Experimental

In the current work, the reactive precipitation of barium sulfate particles was realized with aqueous barium chloride and aqueous sodium sulfate. Barium chloride ($BaCl_2{\cdot}2H_2O$) and sodium sulfate (Na_2SO_4) (analytical grade) were prepared with deionized water, respectively. Sodium pyrophosphate was chosen as the dispersant, added into sodium sulfate, which corresponds to a 10% (w/w) theoretical yield of barium sulfate products. In order to remove solid impurities, all solutions were filtered with filter prior to the storage in containers.

The schematic diagram of experimental setup is shown in **Figure 2(a)**. Experiments were carried out in a Taylor-Couette reactor. It consists of two coaxial cylinders, where the plexiglass outer cylinder keeps static and the aluminum alloy inner cylinder rotates. The dimensions of the Taylor-Couette reactor employed in this study are described in **Table 1**, where the radius ratio is $\eta = r_i/r_o = 40.19/50.00 = 0.80$ and the aspect ratio is $\Gamma = L/\delta_{eq} = 300.00/9.81 = 30.58$. The total volume that can be used for reaction is 922 mL. According to Soos et al.'s study [38], the use of lobed inner cylinder can eliminate or reduce low velocity or shear rate regions, thus improving mixing and mitigating the segregation of particles with different size and density. Therefore, a lobed inner cylinder was chosen for current study. The cross-section profile of both cylinders is shown in **Figure 2(b)**. Due to the feature of lobed inner cylinder, the radius of the inner cylinder will change along the circumferential direction of the cylinder and an equivalent radius based on Eq. (16) is used for evaluation of the gap between the inner and outer cylinders, i.e.,

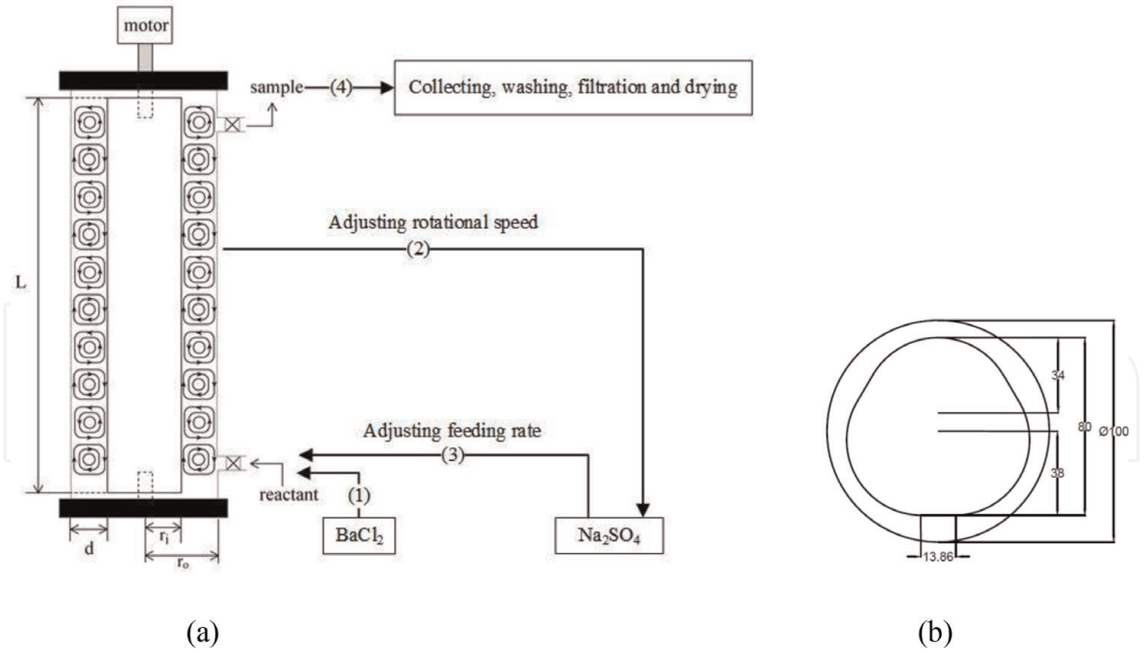

Figure 2.
(a) Schematic diagram of experimental setup for barium sulfate reactive precipitation in a Taylor-Couette flow reactor with the lobed inner cylinder; and (b) cross-section profile of both outer and inner cylinders.

Equivalent radius of lobed inner cylinder, r_i (mm)	40.19
Radius of outer cylinder, r_o (mm)	50.00
Gap size, δ_{eq} (mm)	9.81
Reactor length, L (mm)	300.00

Table 1.
Dimensions of Taylor-Couette reactor.

$$\delta_{eq} = \frac{2A_i}{R_i} \tag{16}$$

where A_i is the cross sectional area of the inner cylinder, and R_i is the perimeter.

All experiments were conducted at room temperature of 20°C. Barium chloride served as the bulk solution, which was fed into the reactor firstly at the bottom of the reactor before the precipitation reaction takes place by peristaltic pump. The rotational speed of the inner cylinder was controlled by a servo motor, and feeding rate was well-controlled by a constant flow peristaltic pump. They have been carefully calibrated before the experiments. After the rotational speed was adjusted to a particular value, the flow was gradually developed to become steady and the feeding rate of tank solution, sodium sulfate was also adjusted to a required value and was then pumped into the reactor to induce the reaction.

Three parameters were involved in these experiments, including rotational speed, feeding rate, and supersaturation. Two initial concentrations (i.e., two supersaturations) of reactants were prepared at 0.1 and 1 mol/L, respectively. At low concentration, rotational speed had a wide range from 25 to 1000 rpm, and feeding rate changed from 5 to 80 mL/min. In total, 49 runs were carried out. At high concentration, rotational speed varied from 50 to 1000 rpm, and feeding rate changed from 5 to 60 mL/min. There were 32 runs were carried out. All parameters and their values have been summarized in **Table 2**. In addition, in order to ensure the repeatability of the experiments, some of the experiments were repeated at least two times.

	c_{BaCl_2} (M)	$c_{Na_2SO_4}$ (M)	Rotational speed (rpm)	Feeding rate (mL/min)
			25	5, 10, 15, 20, 40, 60, 80
			50	5, 10, 15, 20, 40, 60, 80
			100	5, 10, 15, 20, 40, 60, 80
Low concentration	0.1	0.1	300	5, 10, 15, 20, 40, 60, 80
			600	5, 10, 15, 20, 40, 60, 80
			800	5, 10, 15, 20, 40, 60, 80
			1000	5, 10, 15, 20, 40, 60, 80
			50	5, 10, 40, 60
			100	5, 10, 40, 60
			200	5, 10, 40, 60
High concentration	1.0	1.0	300	5, 10, 40, 60
			400	5, 10, 40, 60
			600	5, 10, 40, 60
			800	5, 10, 40, 60
			1000	5, 10, 40, 60

Table 2.
Operating conditions.

During each experiment, suspension samples were taken continuously from the outlet located at the top of the reactor, and at the end of each run they were quickly diluted with deionized water to quench the reaction. After conducting each experiment, the reactor was cleaned by diluted hydrochloric acid to remove barium sulfate particles that have stuck on the wall of the reactor, then rinsed twice with deionized water. Collected samples were washed three times to sufficiently dissolve sodium chloride co-produced in the reaction and other excessive ions. Products were then filtered with mixed cellulose ester microporous membrane filter (pore size 0.22 μm), dried in the oven at 100°C for 24 hours. For even smaller particles, a 0.1 μm pore filter paper was used. Selected samples were then analyzed by SEM (Scanning Electron Microscope). Before taking the SEM observation, the samples were slightly ground. In order to increase the electrical conductivity, silicon wafer was stuck onto carbon tape. Barium sulfate particles were dispersed into ethanol, then dropped on the surface of silicon wafer. Prepared samples were dried in the oven about 10 minutes before conducting SEM observation. Particle size was measured and characterized by the software, Image J, which should establish a coordinate system based on the scale in SEM images. For each reaction condition, at least three images were selected, and 200 particles were measured in each image.

5. Results and discussion

As it has been mentioned before, final particle properties are influenced by many factors. With no additional additives in the system, the properties of particles are directly influenced by the surroundings where the crystals create and grow. Feeding rate affects the local amount of the fresh reactant fed to the system per unit time, which reflects the meso-mixing efficiency in the Taylor-Couette reactor. Rotational speed controls the dispersion degree of fresh reactant, bringing the

unpremixed reactants into contact at a molecular level. It reflects the micro-mixing efficiency of the system. Reactant concentration is the other factor that affects the formation of supersaturation of solution, resulting in the supersaturation being the driving force for the local nuclei formation. Thus, it can be suggested that particle morphology will be controlled by at least these three parameters.

The formation of different morphologies results from the mixing behavior throughout the whole nucleation process, while mixing is caused by fluid shear. Fluid shear generating velocity gradient can re-disperse species, and create eddies. Thus, shear has significant effects on fluid behavior, such as mixing and mass transfer. For a laminar flow, shear rate in the gap can be estimated from the derivative of Eq. (13)

$$\mathrm{G} = \frac{-du_\theta}{dr} = \mathrm{A} - \frac{B}{r^2} \tag{17}$$

The lowest shear rate at outer cylinder wall and the highest shear rate at inner cylinder wall at laminar flow are shown in **Table 3**. Due to the narrow gap of Taylor reactor, the shear rate difference between inner cylinder wall and outer cylinder wall is not significant. Therefore, shear rate in Taylor reactor can be seen as uniform, which can be reasonably expressed by the average shear rate. This feature is also one good performance of this reactor. However, when fluid becomes turbulent, shear rate is not only dominated by tangential velocity due to the enhanced radial and axial velocities induced by Taylor vortex. Also azimuthal velocity is different from the one at laminar state. For turbulent Taylor vortex flow, the local shear rate caused by turbulent eddies with Kolmogorov length scale can be estimated from turbulent energy dissipation rate, given by

$$\mathrm{G} = \sqrt{\frac{\varepsilon}{\nu}} \tag{18}$$

The exact turbulent energy dissipation rate is difficult to determine but the mean turbulent energy dissipation can be estimated from the following equation for Taylor-Couette reactor [26].

$$\langle \varepsilon \rangle = \frac{P}{m_l} = \frac{\pi L r_i^4 \omega_i^3 f}{V} \tag{19}$$

In addition, the friction factor f is given as a function of δ_{eq}/r_i and the Reynolds number [39].

$$\mathrm{f} = 0.80\left(\frac{\delta_{eq}}{r_i}\right)^{0.35} Re^{-0.53} \tag{20}$$

Rotational speed (rpm)	Inner cylinder wall shear rate (s^{-1})	Outer cylinder wall shear rate (s^{-1})	Average shear rate (s^{-1})
25	12.17	9.56	10.87
50	24.35	19.11	21.73
100	48.70	38.23	43.46

Table 3.
Shear rate in laminar Taylor-Couette flow system.

The change of shear rate at different rotational speed for current study is shown in **Figure 3**. It can be seen from **Figure 3** that shear rate has a sharp increase when the flow pattern changes from laminar flow into turbulent flow.

5.1 Particle morphology at a low concentration of 0.1 mol/L

At a low concentration of 0.1 mol/L, the rotational speed was varied from 25 to 1000 rpm with the feeding rate being given ranging from 5 to 80 mL/min. There were three kinds of particle morphology observed from the SEM images in the same magnification as shown in **Figure 4**. The appearance of these particles looks like flake, transition mode and granule, respectively. **Figure 5(a)** shows the changes of morphology under the influence of the rotational speed and feeding rate. The obtaining of the transition mode particles was marked by connecting those data points that can be clearly distinguished from the other two states. It can be seen from the **Figure 5(a)** that the flake particles are mainly formed at low rotational speed while granule particles tend to be presented with the increase of rotational speed at low feeding rate. It is thus indicated from **Figure 5(a)** that the flake particles are expected to be generated when applying the high feeding rate (the top left region of line AB) and granule particles are formed with the high rotational speed (the bottom right region of line DE). However, it cannot be identified that whether or not there exists an intersection point with the development of line AB and line DE.

It has been suggested that beyond a transition Reynolds number at $Re_T = 1.3 \times 10^4$, the flow in the reactor becomes turbulent Taylor flow [40], this corresponding to the rotational speed of 313 rpm (with the aspect ratio $\Gamma = 30.58$) in current study. From **Figure 5(a)**, transition state appears at the rotational speed of 300 rpm, which is in a good agreement with the transition to turbulent Taylor flow as predicted.

5.1.1 Mechanism of granule particles formation

The formation of granule particles with high rotational speed can be explained in terms of the mixing efficiency and agglomerative bonding force. It can be seen from **Figure 5(a)** that the minimum value of rotational speed at which granule particles appear is 600 rpm, and the flow has already developed into fully turbulent Taylor flow. Also, the feeding rate is low enough to form granule particles at this point. As micro-mixing of the fresh feed and bulk solution has significant effects on the final products, the mixing process of two solutions can be explained by the micro-mixing

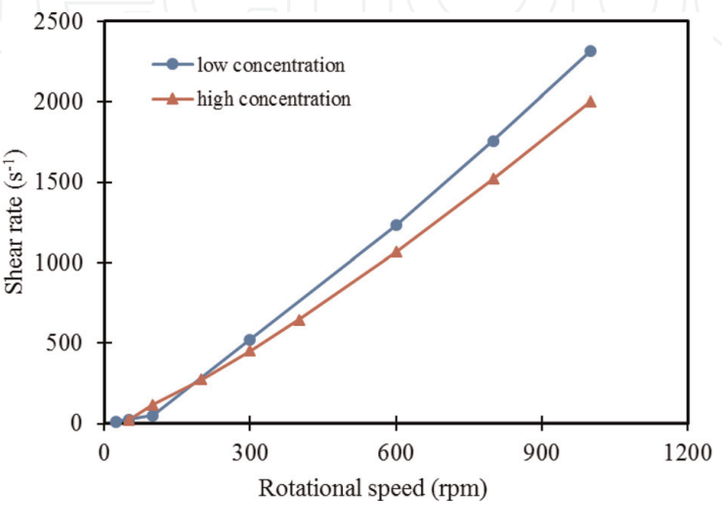

Figure 3.
Shear rate at different rotational speeds.

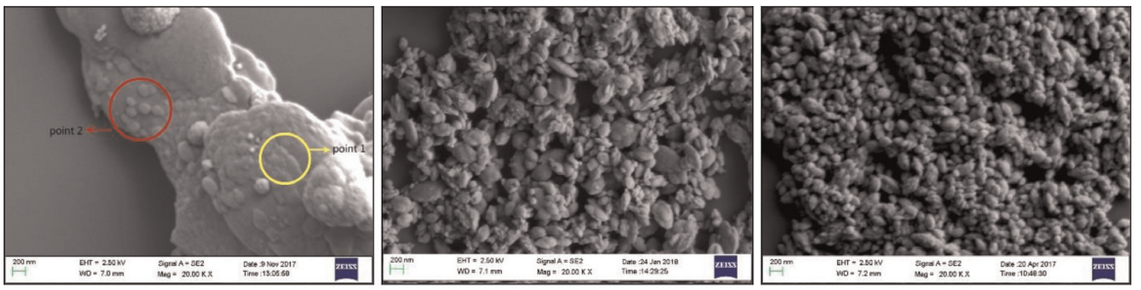

Figure 4.
Three representative morphologies of barium sulfate particles at low concentration. (a) ω = 25 rpm; Q = 20 mL/min, flake; (b) ω = 300 rpm; Q = 40 mL/min, transition; and (c) ω = 600 rpm; Q = 5 mL/min, granule.

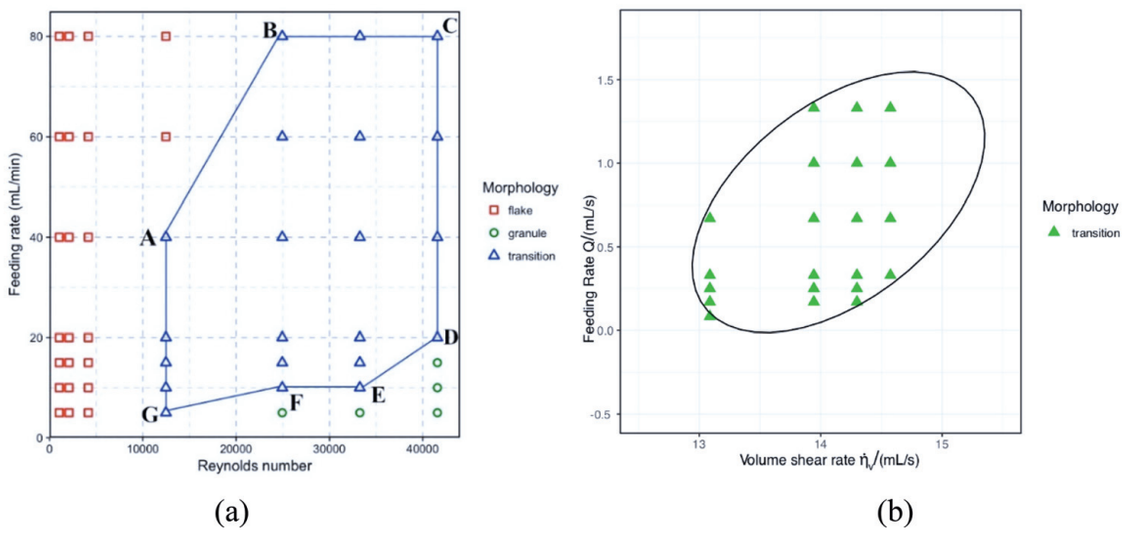

Figure 5.
(a) Morphology distribution at various rotational speed (Reynolds number) and feeding rate at low concentration; (b) Morphology distribution for transition status where the transition boundary has been marked by curve fitting.

model. Many theoretical models have been proposed to describe the micro-mixing behavior in the reactors, such as diffusion model [41], deformation-diffusion model [42], eddy engulfment model [21], and incorporation model [43]. Among these models, the engulfment model proposed by Baldyga and Bourne [21] has been widely adopted. The engulfment rate is defined as

$$E = 0.058\left(\frac{\varepsilon}{\nu}\right)^{1/2} \tag{21}$$

Based on this model, two species are considered as two shrinking slabs [15]. In case of turbulent Taylor vortex flow, once the fresh reactant Na_2SO_4 has been added into the Taylor-Couette flow reactor, two reactant slabs are in contact and interact each other with the turbulent eddies being stretched due to turbulent vorticity and generating a local turbulent shear. The scale of eddies can be approximately considered as being proportional to Kolmogorov length scale, defined by

$$\lambda_{eddy} = C_{eddy}\left(\frac{\nu^3}{\varepsilon}\right)^{1/4} \tag{22}$$

Fluid velocity fluctuation increases with intensified turbulence. More small eddies generate and dissipate. It can be seen from Eq. (22) that the length scale is

reduced with the increase of energy dissipation rate. The incorporation of fresh feed after finishing the processes of engulfment and deformation will finally become small fluid elements, smaller than Kolmogorov length scale. Accordingly, at high rotational speed, the contact area between fresh solution and bulk solution increases, leading to the acceleration of the molecular diffusion. The characteristic diffusion time can be estimated according to Baldyga and Bourne [44], given by

$$t_D = 2\left(\frac{\nu}{\varepsilon}\right)^{1/2} arcsinh(0.05S_C) \tag{23}$$

where *Sc* is Schmidt number. Based on this model, the characteristic time by engulfment on the course of mixing is roughly equal to E^{-1},

$$t_m = 12\left(\frac{\nu}{\varepsilon}\right)^{1/2} \tag{24}$$

In our experiment, this characteristic time (estimated to range from 0.711 to 0.0075 s based on different rotational speed) was about 17 times larger than diffusion time (estimated to range from 0.041 to 0.0004 s). Therefore, it is suggested that the engulfment may control the micro-mixing process which can be seen as the rate-determining step and t_m can be seen as the typical micro-mixing time.

The time constants are of importance in assessing the influence of mixing on reactive precipitation. It has been suggested by Baldyga and his co-workers [23] that when the mixing time, t_m is shorter than the induction time t_N, $t_m < t_N$, nucleation step cannot be affected by mixing intensity, as the local region has uniformly dispersed with reactants before nucleation. While when $t_m > t_N$, nucleation would occur in a non-uniform region. Under this condition, the effect of mixing on precipitation can be crucial. Since the $BaSO_4$ reactive precipitation is fast by nature, reactants contact quickly once the Na_2SO_4 has been added into the Taylor-Couette flow reactor, resulting in the generation of local supersaturation. Then, nuclei are formed in the duration of induction. The induction time was about 0.0014 s, which was smaller than the micro-mixing time 0.0075 s at 1000 rpm. Therefore, reactive precipitation can be controlled by mixing condition achieved by fluid shear. Because the induction period is independent with the micro-mixing process, the precipitation reaction takes place and the rest of fresh reactants is incorporated and diffused into the vortices at the same time. Therefore, the maximum nucleation rate attains at the first contact of two species due to the dilution of supersaturation. This in fact indicates that after a number of nuclei are formed, the growth rate decreases with the reduced supersaturation as there is little amount of reactant left for nuclei to grow further.

At the end of the primary process of crystallization, secondary process takes place, having a determining effect on particle qualities. Nuclei grow into grains then crystallites. This process is dependent on the mass transfer, while mass transfer is caused by interfacial concentration gradient. Convective mass transfer and diffusive mass transfer coexist in the system simultaneously. Here the Sherwood number, *Sh* derived by Armenante and Kirwan [28] as a function of Reynolds number and Schmidt number can be used to illustrate the interfacial mass transfer during nuclei growth.

$$Sh = 2 + 0.52Re^{0.52}Sc^{1/3} \tag{25}$$

As granule particles are formed at a relative high rotational speed, an increase in Sherwood number indicates an enhanced convection mass transfer from bulk solution to solid surface. It can be deduced that an intensified interfacial mass transfer can facilitate the formation of granular particles. Additionally, Peclet number, *Pe* is

used here to determine the dominant effect on the interaction among particles, expressed as a function of Reynolds number and Schmidt number which is given by

$$P_e = R_e S_C = \frac{r_i \omega_i \delta_{eq}}{D} \tag{26}$$

where D is the diffusion coefficient, including the effects of Brownian motion and molecular diffusion. The range of Pe applicable in the present experiments was $9.7 \times 10^5 < Pe < 3.9 \times 10^7$, which was much greater than 1 ($Pe >> 1$). Larger Pe values indicate that the particle collision is dominated by the convective mass transfer due to Taylor turbulent eddy transport. Such convection effect can also be improved by the intensification of turbulent eddies, realized by increasing the rotational speed of the inner cylinder.

Due to the entrainment of these crystallites by the turbulent eddies, the self-assembled aggregation makes them closer, leading to the agglomeration of crystallites which further results in the formation of final particles. In Aljishi et al.'s study [6], they described crystallites as the primary grains and final particles as the secondary grains. The joint effect of micro-mixing and crystallization on the formation of the particles and its mechanism are illustrated in **Figure 6**. For powder-like particle preparation, agglomeration becomes an important growth mechanism due to a large number of nuclei created. The final particle morphology is a result of the relative rates of chemical reaction, nucleation, growth and agglomeration. During this process, the motion of two or more crystallites in suspension makes them closed and then aggregate. Furthermore, once the crystals have stayed together for a sufficient long time, the agglomerative bonds can be formed due to intergrowth [45]. An empirical formulation of the net agglomeration rate (including bond making and breaking) was proposed

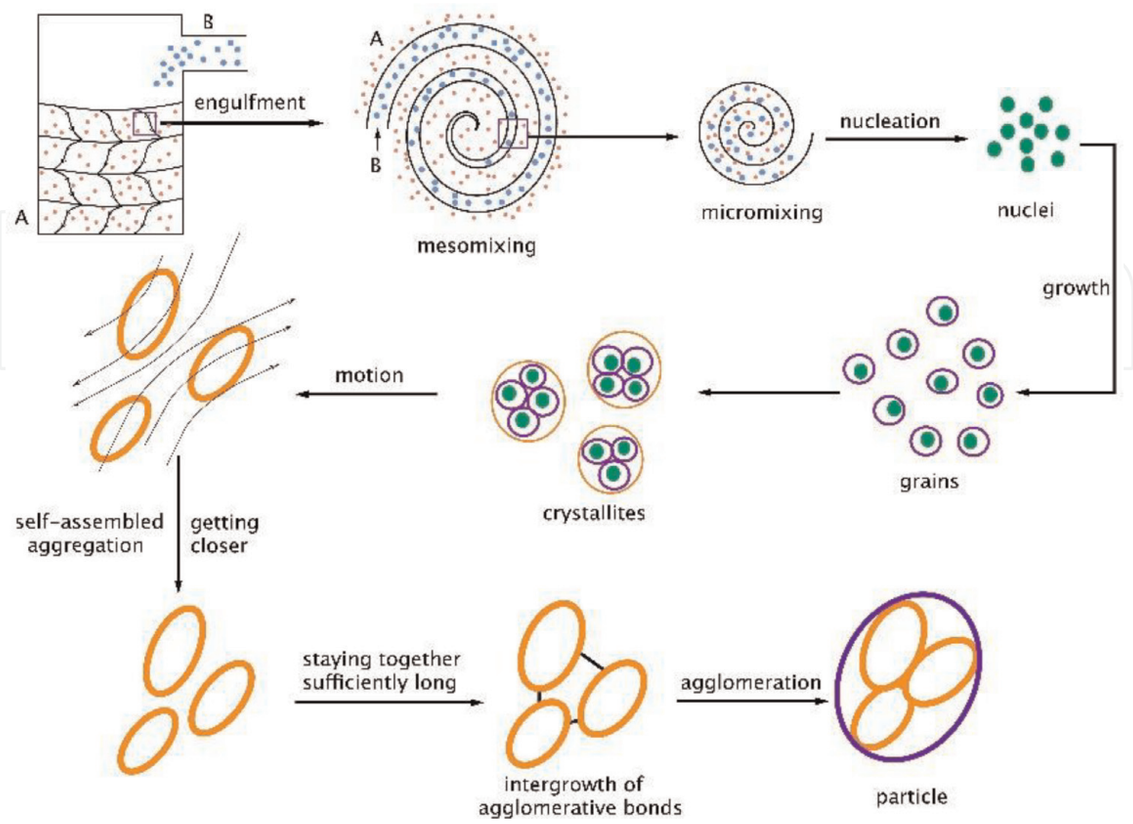

Figure 6.
Mechanism of particle formation in fluid.

$$K_{aggl} = \beta_{aggl} \epsilon^p S^q f(l_m, l_n) \tag{27}$$

where β_{aggl} is agglomeration efficiency, l_m and l_n denote the sizes of the binary agglomerating particles. It can be seen clearly from this equation that the agglomeration rate is influenced by the turbulence dissipation rate and supersaturation. Therefore, for a given rotational speed, the average shear rate is a constant while along with the nucleation process based on our analysis before, the supersaturation is reduced. This can then result in the reduction of agglomeration rate. Accordingly, the particle size cannot increase continuously as the agglomeration rate reaches its limit at a given condition. This is consistent with the results obtained in the experiments. At the granule state, particles morphologies are similar and their size were kept at around 180 to 200 nm no matter the change of rotational speed. This result is consistent with the finding of Dehkordi and Vafaeimanesh [46]. They also obtained a constant final particle size. Moreover, especially at high rotational speed of 1000 rpm, application of the higher feeding rate can still promote the generation of granule particles because at this feeding rate, the mass dispersed is saturated while the reaction process remains the same, thus resulting in the particle size unchanged. This can explain why the particle morphologies and sizes are similar at granule state no matter how the feeding rate and rotational speed change.

In addition, at transition state, we also measured the particle size, and found that the particle size exhibits a reduction trend with increase in the rotational speed at a constant feeding rate as shown in **Figure 7**. Based on the Reynolds number calculated before, at the rotational speed of 300 rpm, turbulent Taylor vortex flow has been formed. Particle morphology shows a significant difference from the previous large blocks with irregular shape. The rotational speed of 300 rpm almost corresponds to the point where turbulent Taylor vortex flow began to form. Thus, the disturbance effect of feeding rate cannot be ignored. Fluid is sensitive to any small perturbation, as this perturbation will lead to big velocity fluctuation, then create small eddies. Aljishi et al. [6] observed in their experiment that with increase in axial flow intensity, the onset of flow pattern instability is significantly delayed. Also, it can be seen from **Figure 5(a)** that at 600 rpm, the beginning point of granule particles formation are observed at a low feeding rate, where the disturbance effect is weak. Therefore, it is suggested that the appearance of particle size reduction trend can be seen as an indicator for morphology transition.

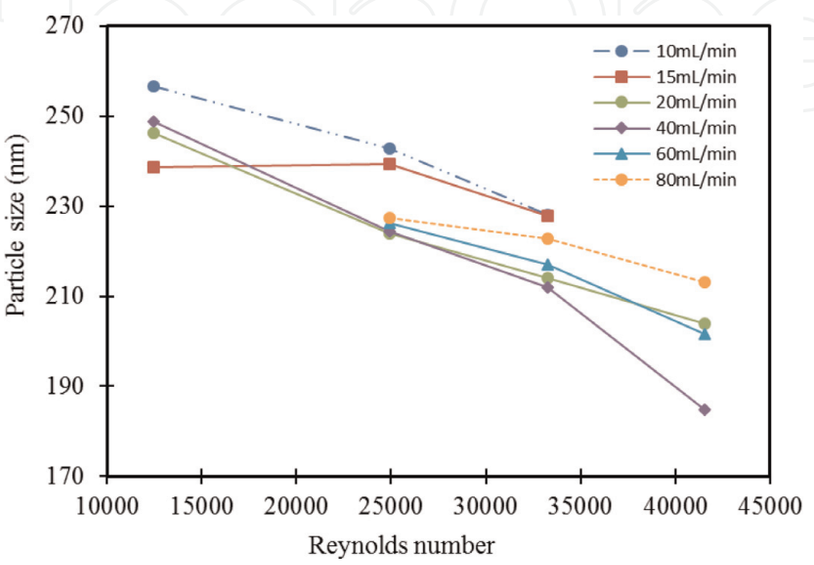

Figure 7.
Change of particle size with rotational speed (Reynolds number) at transition state at low concentration.

5.1.2 Mechanism of the formation of flake particles

It can be clearly seen from **Figure 4(a)** that the formation of big flake particles resulted from the stable agglomeration of smaller particles. The blurred boundary marked at point 1 and the small particles attached at point 2 indicate that the big flake particle is the product of small particles aggregation then agglomeration or level by level accumulation. This formation process is strongly influenced by the flow dynamics. In order to elaborate on this phenomena, **Figure 8** shows the morphology of the formed flake particles at various rotational speeds. **Figure 8(e)** also shows the transition mode particles for comparison.

Firstly, many small particles are formed and suspend in the mixture solution. When low rotational speed is applied, the entrainment on the fresh feed by eddies is not strong and the formed particles can disperse quite uniformly. Because at laminar state, velocity is dominated by azimuthal velocity. The effect of Taylor vortex is not significant. Therefore, mixing behavior is not strong. Accordingly, the contact area between the bulk solution and the fresh feed is not big enough instead more mass transfers to the formed small particle surface, leading to the local accumulation. The length scale of particles is smaller than minimum vortex scale. Fluid shear induced by the velocity gradient acted on particle agglomeration. Therefore, the small particles generated under this condition are still larger than those in high rotational speed. Also, weak shear decreases the engulfment of bulk solution and fresh feed, which means the exchange between the bulk solution entrained by eddies and fresh feed is poor at the inlet. This phenomenon becomes notable at a high feeding rate. For a particular small region, enhanced collision can promote the generation of agglomeration bonds. This kind of agglomeration is gradually reduced as shown from **Figure 8(b)–(e)**, consistent with the analysis above. It should be noted that as can be seen from **Figure 8(a)** where there is no influence of the turbulent eddies due to zero rotational speed of the inner cylinder, few formed small particles can be still observed. At this condition, the droplets of fresh Na_2SO_4 feed directly contact with bulk $BaCl_2$ solution from the inlet and are diffused into the bulk solution, the reactive product as agglomerated big flakes sinks to the

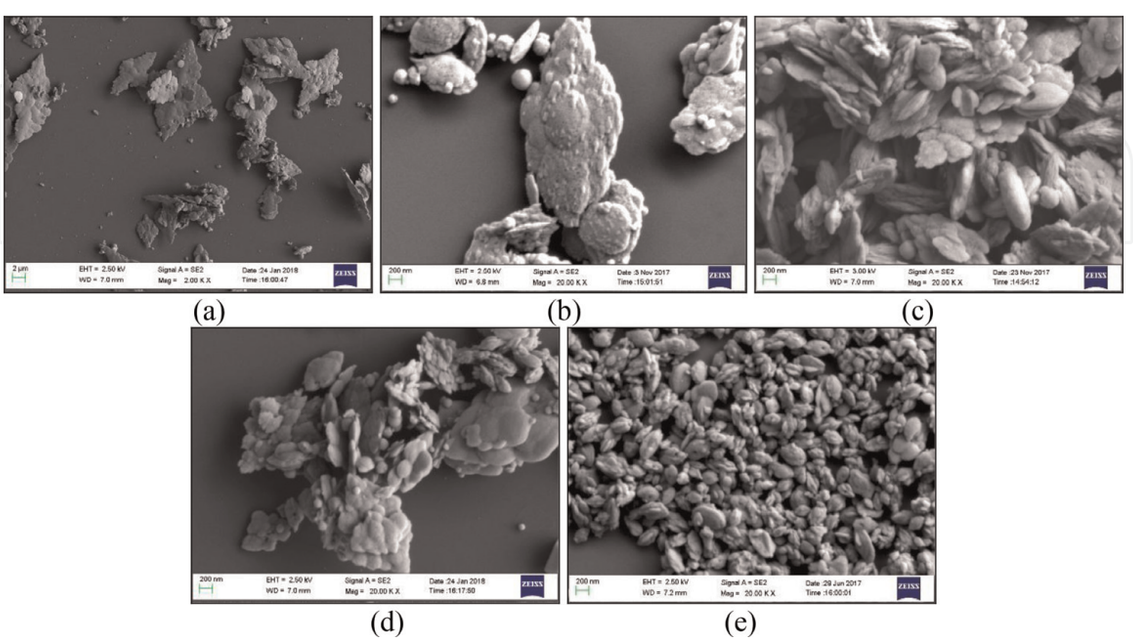

Figure 8.
Development of the flake particles with increase of the rotational speed. (a) ω = 0, flake; (b) ω = 25 rpm, flake; (c) ω = 50 rpm, flake; (d) ω = 100 rpm, flake; and (e) ω = 300 rpm, transition. Note: the magnification of image (a) is 2.00 k, and the others are 20.00 k.

bottom of reactor. This is likely caused by a local saturated diffusion in which many formed small particles agglomerate to form the big flakes.

Secondly, the effect of eddy shear on flake particles is different from granule particles. At high rotational speed, micro-mixing takes place at Kolmogorov length scale, which is larger than the size of granule particles. Therefore, larger turbulent eddies only affect the mixing process of two species, indicating that the particles passively follow the vortex motion. Here we use Stokes number, *St* to describe the trapping of particles by an eddy [47].

$$\mathrm{St} = \frac{\rho_p d^2 u_t}{18\mu l} \tag{28}$$

where u_t is the terminal velocity of particles [48], and l is the suitable length scale for the vortex. For small eddies in Taylor reactor, l can be chosen as Kolmogorov length scale for the calculation of St. At high rotational speed for the formation of granule particles with the diameter of 200 nm, *St* is approximately 1.1×10^{-9}, which is much smaller than 1.0. As indicated by Crow et al. [42], $St << 1.0$ represents the case that particles are well following the eddy. However, for low rotational speed, Kolmogorov length scale increases, and the scale of formed flake particles is in the order of eddies. Vortex and flake particles are all at micron scales. Therefore, eddy shear strongly interacts with the flake particles. If shear force is strong enough, the size of flake particles will be smaller than Kolmogorov length scale as the particle surface will be ripped off. This is consistent with the observation from the semi-batch precipitation experiment of Baldyga et al. [15] in which they suggested that rotational speed had no influence on particle size at a relatively weak turbulence. Barresi et al. [12] also agreed with this argument from their variation coefficient analysis.

Based the analysis above, both rotational speed and feeding rate have effects on final particle morphology. Also, the transition region in **Figure 5(a)** indicates an ellipse-like shape when the both parameters are combined. In order to obtain quantitative information about particle morphology, a fitting equation is proposed involving shear rate (rotational speed) and feeding rate, shown in **Figure 5(b)**.

$$0.33\dot{\eta}_V^2 - 0.51\dot{\eta}_V Q + 0.79Q^2 - 9.06\dot{\eta}_V + 6.02Q + 61.41 = 0 \tag{29}$$

The relationship is expressed in a semi-natural log coordinate. In order to unify the dimension, shear rate here refers to the entire volume shear rate, $\dot{\eta}_V$ for the Taylor reactor, defined as.

$$\dot{\eta}_V = GV \tag{30}$$

Eq. (28) can be seen as an indicator for particle morphology. Inside the ellipse, transition mode takes place, while in the top left region of the ellipse, flake particles can be created, and in the bottom right region, granule particles are formed.

5.2 Particle morphology at a high concentration of 1.0 mol/L

In order to elaborate on this transition phenomenon, experiments at a higher concentration of 1.0 mol/L were also carried on. The rotational speed was varied from 50 to 1000 rpm, and the feeding rate was changed from 5 to 60 mL/min. Three similar morphologies as at low concentration were observed as shown in **Figure 9**.

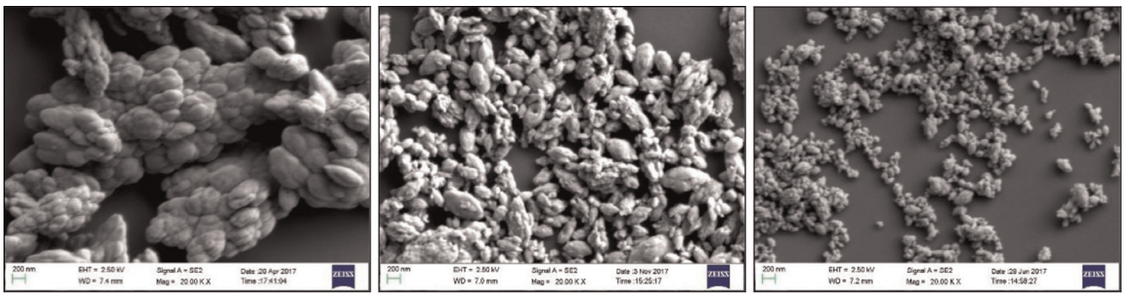

(a) (b) (c)

Figure 9.
Three representative morphologies of barium sulfate particles at high concentration. (a) ω = 50 rpm; Q = 5 mL/min, flake; (b) ω = 100 rpm; Q = 5 mL/min, transition; and (c) ω = 800 rpm; Q = 10 mL/min, granule.

Also, a transition region was identified to distinguish the other two states as shown in **Figure 10**. Compared with that shown in **Figure 5(a)** at 0.1 mol/L, the transition region is exhibited to be narrower while the beginning points and ending points fall into the range of relatively lower rotational speeds. Particle size at transition state were measured, also illustrating a reduction trend as shown in **Figure 11**. Thus, the size reduction can be considered as an indicator for morphology transition.

At low concentration, the change of kinematic viscosity means the change of Reynolds number even at the same rotational speed. The kinematic viscosity at 1.0 mol/L is about 1.85 times as high as 0.1 mol/L. According to the radius ratio of $\eta = 0.80$, the critical Reynolds number to generate Taylor vortex flow is 97.33 [34]. The generation of turbulent Taylor vortex flow is at a Reynolds number ratio of $R = Re/Re_c \sim 35$ as indicated by Bubakova et al. [29], corresponding to the rotational speed of 89 rpm. Therefore, turbulent Taylor vortex flow occurs at the rotational speed of 89 rpm, roughly corresponding to the beginning of transition state at 100 rpm in this case. Also, fully turbulent flow is formed at the rotational speed of 581 rpm, roughly corresponding to the ending of transition state with the rotational speed of 600 rpm. We thus deduce that the morphology transition is correlated with the flow patterns in the reactor. Based on engulfment model, a good mixing of

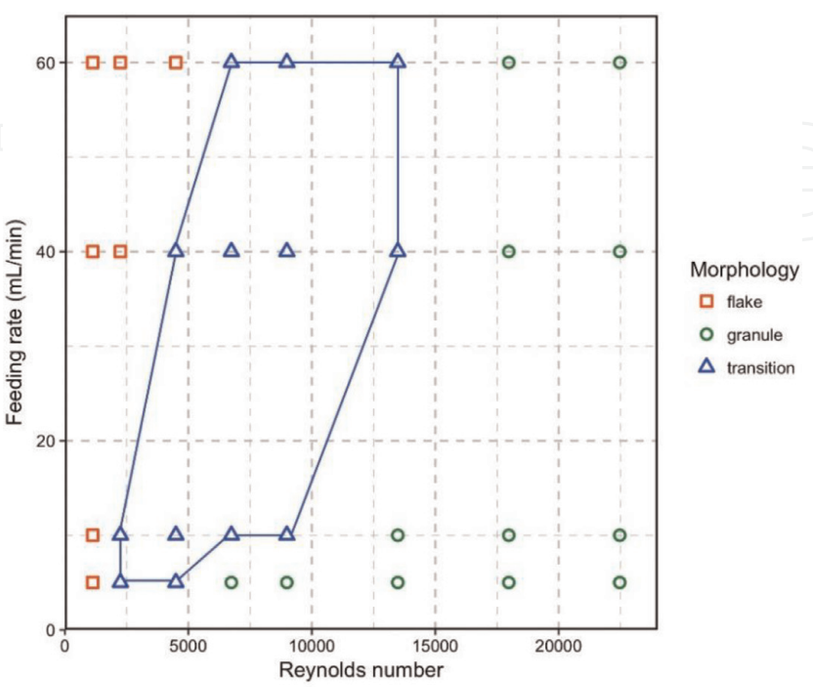

Figure 10.
Morphology distribution at various rotational speed (Reynolds number) and feeding rate at high concentration.

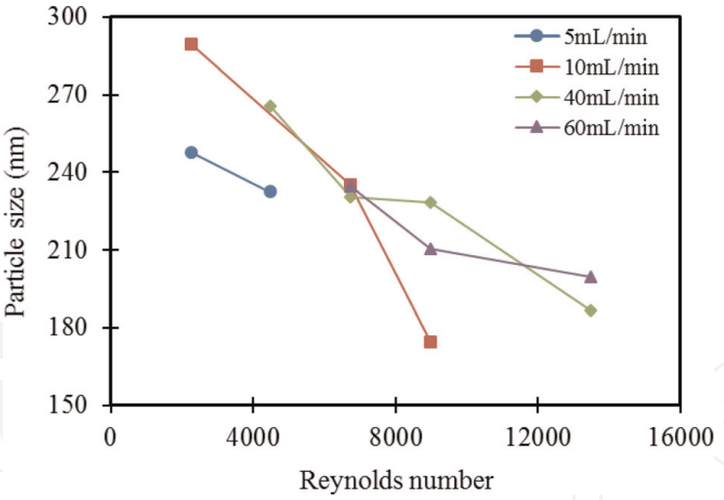

Figure 11.
Change of particle size with rotational speed (Reynolds number) at transition state at high concentration.

two species needs high energy input. As mentioned earlier, formation of flake particles is the result of the poor dispersion of reactants. When the transition was observed, the micro-mixing was improved. In the present work, the transition state was observed at least under the condition of turbulent flow.

5.3 Influence of the low concentration and high concentration on particle formation

It was noticed that the onset of the transition state is different for different concentrations. At low concentration, transition state was observed at turbulent flow regime at 300 rpm while at high concentration, such transition appears at turbulent Taylor vortex flow regime at 100 rpm. Also, the transition range becomes smaller at high concentration. To keep the Reynolds number unchanged, the increase in kinematic viscosity means that the rotational speed has to be increased to maintain the same fluid pattern. This implies that the transition state should be observed at a higher rotational speed than that in low concentration. Also, based on the mechanism of various morphologies formation at low concentration, the onset of turbulent flow is essential for the creation of transition particles. However, at high concentration, transition state appeared at a much lower rotational speed. The final granule particle size at high concentration was approximately measured as 130–150 nm, which is smaller than that at low concentration.

The above observed results should also result from the increase in local supersaturation, which was the only varying parameter in the comparison experiments. Since the nucleation and growth are directly dependent on supersaturation, the effect of supersaturation is crucial on morphology transition. As can be seen from Eqs. (10) and (11), the order of magnitude of nucleation rate is much higher than growth rate, indicating that nucleation is more sensitive to supersaturation than growth. Many studies have been suggested that an increase in supersaturation may result in the nucleation process to be dominant [12]. In the experiments of Barresi et al. [12] and Marchisio et al. [13], they all observed tabular particles to form at low concentration and dendritic particles at high concentration. Baldyga et al. [15] suggested that the formation of tabular shape is the consequence of surface nucleation, leading to the overgrowth of crystal surface. While with improvement of flow environment (increasing flow rate in jet) round-shaped particles can form [13]. In our experiment, granule particles were observed with the increase of the rotational speed (likely corresponding a strong local turbulent shear due to the turbulent

eddies). Since with the increase in supersaturation, the mass brought into the system is more than that at low supersaturation for the same small droplets. In such environment, the available reactant molecules mainly function to form nuclei. Thus, the nucleation significantly increases. It is thus concluded that a higher nucleation rate facilitates the creation of a large number of nuclei which is beneficial to the formation of small particles. On the other hand, as mentioned in the part 5.1.1, an increased interfacial concentration gradient can facilitate the formation of granular morphology. Therefore, in general, a high supersaturation results in the formation of small granule particles. It should be noticed that agglomeration is an important part on the course of nucleation. It is usually significant at low mixing rate [46]. At low rotational speed, agglomerative bonding force is strengthened due to weak shear and large vortex scale, more primary crystallites agglomerate to form large flake particles as discussed earlier. It can thus be inferred that the supersaturation can be seen as a primary factor in determining particle morphology while the effect of agglomeration is the second place but it cannot be ignored at low rotational speed. Furthermore, from the analysis of particle formation mechanism mentioned above, the creation of agglomerative bonds requires a close distance and sufficient long time. With the increase of rotational speed, fluid motion becomes more significant. The formation of agglomerative bonds was reduced, followed with the number decrease of crystallites to agglomerate. Therefore, it is suggested that the appearance of particle size reduction trend can be seen as an indicator for morphology transition.

Based on the analysis and discussion above, it can be suggested that when using Taylor-Couette flow reactor for synthesis of the particles, mixing affects the whole process especially for the mixing of individual reactant solution through the engulfment and the subsequent chemical reaction. Supersaturation has the effect on crystallization process when reactants are in contact but this effect may surpass the flow environment. It is conjectured that agglomeration can be seen as a consequence of flow dynamics and supersaturation when working on crystallites. Last but not the least, interfacial phenomenon between liquid and solid particles exists throughout the whole precipitation process. It includes mainly two aspects. One is from the interfacial concentration distribution, which determines the mass transfer process from liquid to solid, thus nuclei growth process, and the other is the surface treatment of fluid shear on final agglomerates.

6. Conclusions

In the present work, a Taylor-Couette reactor was employed for the purpose of controllable production of barium sulfate particles with various morphologies. The morphologies obtained include flake particles, transition particles and granule particles. During the reactive precipitation process, three main control parameters were assessed. The presence of a particular morphology results from the combined effect of these parameters. For different solution conditions, the influence of fluid dynamic environment inside the Taylor-Couette reactor on particle morphology may change. In general, morphology transition is suggested to be related to the change of flow pattern that the turbulent eddies strongly interact with the particle crystals. Considering the joint effect of fluid dynamics and supersaturation, it can be deduced that micro-mixing caused by fluid shear plays a primary role in species dispersion, which determines the formation of various morphologies, while the supersaturation controls the crystallization process, which determines the onset of transition state. Both fluid shear and supersaturation can finally affect the interfacial concentration distribution, thus particle growth. Then particle agglomeration

can be controlled by interfacial shear force. It is thus concluded that interfacial phenomenon plays significant roles in the transition of particle morphologies during precipitation. More specifically, the following conclusions have been drawn from the current study:

1. At low supersaturation, the morphology transition mode is observed at fully developed turbulent Taylor flow, and it appears at turbulent Taylor vortex flow at high concentration. It is indicated that turbulent shear creating isotropic small eddies can assist controllable synthesis of particles, which results in the generation of relatively regular morphology. This is due to the enhanced mixing intensity and interfacial mass transfer caused by shear at turbulent flow. However, anisotropic vortex shear in laminar state has the potential to create irregular particle morphology. On the other hand, agglomeration as a part of crystallization, can be enhanced by both low mixing intensity and high supersaturation, leading to the formation of flake particles.

2. The decrease in particle size with the increase of rotational speed at transition state results from the disturbance effect of the feeding rate. Fluid is sensitive to any small perturbation especially at high rotational speed, then more small isotropic eddies will be created.

3. Compared the transition results at both low and high concentrations, supersaturation will lead itself to the formation of smaller particles, and the transition at lower rotational speed. Although the use of high supersaturation can increase the agglomeration for a given rotational speed, it facilitates the formation of a large number of nuclei but leaves little mass for further particle growth. A high interfacial concentration also enhances the mass transfer between fluid and solid particles. Thus, it can be inferred that the supersaturation has a stronger effect than the agglomeration in determining the particle morphology.

Nomenclature

a	ion activity, mol/kg
A_i	cross sectional area of the inner cylinder, m
B	growth rate, m/s
c	molar concentration, mol/L
Δc	concentration difference, mol/L
d	diameter of particle, m
D	molecular diffusion coefficient, m^2/s
E	engulfment rate, s^{-1}
f	friction factor
G	shear rate, s^{-1}
I	ionic strength, mol/kg
J	nucleation rate, m/s
k_{aggl}	agglomeration rate
K_g	total growth coefficient, m/s
K_{sp}	thermodynamic solubility product, mol^2/L^2
l	length scale, m
l_m	size of agglomerating particle m, m
l_n	size of agglomerating particle n, m
L	reactor length, m

n	kinetic order of nucleation
Pe	Peclet number
Q	feeding rate, mL/min
r_i	equivalent radius of the lobed inner cylinder, m
r_o	radius of the lobed outer cylinder, m
R	gas constant, J/(mol·K)
Re	Reynolds number
R_i	perimeter of the inner cylinder, m
S	saturation ratio
Sa	supersaturation ratio
Sc	Schmidt number
Sh	Sherwood number
St	Stokes number
t_D	diffusion time, s
t_N	induction time, s
t_m	micro-mixing time, s
T	absolute temperature, K
u_t	terminal velocity of particle, m/s
u_θ	azimuthal velocity, m/s
V	volume of reactor, m^3
z	charge number

Greek letters

β_{aggl}	agglomeration efficiency
$\gamma_\pm$	activity coefficient
δ_{eq}	equivalent gap, m
Γ	aspect ratio
ε	turbulent energy dissipation rate, m^2/s^2
ζ	angular velocity ratio
η	radius ratio
$\dot{\eta}_V$	volume shear rate, mL/s
λ_{eddy}	eddy length scale, m
μ	viscosity of the fluid, kg/(m·s)
ρ_d	density of particle, kg/m^3
σ	supersaturation
υ	kinematic viscosity of the fluid, m^2/s
φ	molar chemical potential, J/mol
ω_i	rotational speed of the lobed inner cylinder, rad/s

Acknowledgements

This work was financially supported by National Natural Science Foundation of China (NSFC) through the grants (Nos. 21576141, 21606259). This work was carried out at the International Doctoral Innovation Centre (IDIC), UNNC. Lu Liu would also like to acknowledge the support through the Ph.D. scholarship of the International Doctoral Innovation Centre (IDIC) of University of Nottingham Ningbo China.

DOI: http://dx.doi.org/10.5772/intechopen.85647

IntechOpen

Author details

Lu Liu[1,2], Guang Li[1,2], Xiaogang Yang[1,2]*, Xiani Huang[1,2] and Chenyang Xue[1,2]

1 International Doctoral Innovation Centre, University of Nottingham Ningbo China, Ningbo, P.R. China

2 Department of Mechanical, Materials and Manufacturing Engineering, University of Nottingham Ningbo China, Ningbo, P.R. China

*Address all correspondence to: xiaogang.yang@nottingham.edu.cn

IntechOpen

© 2019 The Author(s). Licensee IntechOpen. This chapter is distributed under the terms of the Creative Commons Attribution License (http://creativecommons.org/licenses/by/3.0), which permits unrestricted use, distribution, and reproduction in any medium, provided the original work is properly cited. CC BY

References

[1] Tai CY, Chen FB. Polymorphism of CaCO3, precipitated in a constant-composition environment. AICHE Journal. 1998;**44**(8):1790-1798

[2] Tai CY, Chen PC. Nucleation, agglomeration and crystal morphology of calcium carbonate. AICHE Journal. 1995;**41**(1):68-77

[3] Jung WM, Kang SH, Kim WS, Choi CK. Particle morphology of calcium carbonate precipitated by gas–liquid reaction in a Couette–Taylor reactor. Chemical Engineering Science. 2000; **55**(4):733-747

[4] Akyol E, Cedimagar MA. Size and morphology controlled synthesis of barium sulfate. Crystal Research and Technology. 2016;**51**(6):393-399

[5] Judat B, Kind M. Morphology and internal structure of barium sulfate—derivation of a new growth mechanism. Journal of Colloid and Interface Science. 2004;**269**(2):341-353

[6] Aljishi MF, Ruo AC, Park JH, Nasser B, Kim WS, Joo YL. Effect of flow structure at the onset of instability on barium sulfate precipitation in Taylor–Couette crystallizers. Journal of Crystal Growth. 2013;**373**:20-31

[7] Farahani HB, Shahrokhi M, Dehkordi AM. Experimental investigation and process intensification of barium sulfate nanoparticles synthesis via a new double coaxial spinning disks reactor. Chemical Engineering and Processing: Process Intensification. 2017;**115**:11-22

[8] Wu G, Zhou H, Zhu S. Precipitation of barium sulfate nanoparticles via impinging streams. Materials Letters. 2007;**61**(1):168-170

[9] Nielsen AE. Nucleation in barium sulfate precipitation. Acta Chemica Scandinavica. 1957;**11**:1512-1515

[10] Nielsen AE. The kinetics of crystal growth in barium sulfate precipitation. Acta Chemica Scandinavica. 1958;**12**(5): 951-958

[11] Nielsen AE. The kinetics of crystal growth in barium sulfate precipitation. Acta Chemica Scandinavica. 1959;**13**: 1680-1686

[12] Barresi AA, Marchisio D, Baldi G. On the role of micro-and mesomixing in a continuous Couette-type precipitator. Chemical Engineering Science. 1999;**54** (13–14):2339-2349

[13] Marchisio DL, Barresi AA, Garbero M. Nucleation, growth, and agglomeration in barium sulfate turbulent precipitation. AICHE Journal. 2002;**48**(9):2039-2050

[14] Li J, Liu D, Jiang H, Wang J, Jing X, Chen R, et al. Effects of polyacrylic acid additive on barium sulfate particle morphology. Materials Chemistry and Physics. 2016;**175**:180-187

[15] Baldyga J, Podgórska W, Pohorecki R. Mixing-precipitation model with application to double feed semibatch precipitation. Chemical Engineering Science. 1995;**50**(8):1281-1300

[16] Baldyga J, Orciuch W. Closure problem for precipitation. Chemical Engineering Research and Design. 1997; **75**(2):160-170

[17] Phillips R, Rohani S, Baldyga J. Micromixing in a single-feed semi-batch precipitation process. AICHE Journal. 1999;**45**(1):82-92

[18] Pagliolico S, Marchisio D, Barresi AA. Influence of operating conditions on $BaSO_4$ crystal size and morphology in a continuous Couette precipitator. Journal of Thermal Analysis and Calorimetry. 1999;**56**(3):1423-1433

[19] Thai DK, Mayra QP, Kim WS. Agglomeration of Ni-rich hydroxide crystals in Taylor vortex flow. Powder Technology. 2015;**274**:5-13

[20] Mayra QP, Kim WS. Agglomeration of Ni-rich hydroxide in reaction crystallization: Effect of Taylor vortex dimension and intensity. Crystal Growth & Design. 2015;**15**(4): 1726-1734

[21] Baldyga J, Bourne JR. A fluid mechanical approach to turbulent mixing and chemical reaction Part III computational and experimental results for the new micromixing model. Chemical Engineering Communications. 1984;**28**(4–6):259-281

[22] Vicum L, Mazzotti M, Baldyga J. Applying a thermodynamic model to the non-stoichiometric precipitation of barium sulfate. Chemical Engineering & Technology. 2003;**26**(3):325-333

[23] Baldyga J. Mixing and fluid dynamics effects in particle precipitation processes. Kona Powder and Particle Journal. 2016;**33**:127-149

[24] Li G, Yang X, Ye H. CFD simulation of shear flow and mixing in a Taylor–Couette reactor with variable cross-section inner cylinders. Powder Technology. 2015;**280**:53-66

[25] Brian PLT, Hales HB, Sherwood TK. Transport of heat and mass between liquids and spherical particles in an agitated tank. AICHE Journal. 1969; **15**(5):727-733

[26] Kuboi R, Komasawa I, Otake T. Behavior of dispersed particles in turbulent liquid flow. Journal of Chemical Engineering of Japan. 1972; **5**(4):349-355

[27] Garside J, Jančić SJ. Growth and dissolution of potash alum crystals in the subsieve size range. AICHE Journal. 1976;**22**(5):887-894

[28] Armenante PM, Kirwan DJ. Mass transfer to microparticles in agitated systems. Chemical Engineering Science. 1989;**44**(12):2781-2796

[29] Bubakova P, Pivokonsky M, Filip P. Effect of shear rate on aggregate size and structure in the process of aggregation and at steady state. Powder Technology. 2013;**235**:540-549

[30] Debye P, Hückel E. De la theorie des electrolytes. I. abaissement du point de congelation et phenomenes associes. Physikalische Zeitschrift. 1923;**24**(9): 185-206

[31] Dirksen JA, Ring TA. Fundamentals of crystallization: Kinetic effects on particle size distributions and morphology. Chemical Engineering Science. 1991;**46**(10):2389-2427

[32] Carosso PA, Pelizzetti E. A stopped-flow technique in fast precipitation kinetics—the case of barium sulphate. Journal of Crystal Growth. 1984;**68**(2): 532-536

[33] Wereley ST, Lueptow RM. Spatio-temporal character of non-wavy and wavy Taylor–Couette flow. Journal of Fluid Mechanics. 1998;**364**:59-80

[34] DiPrima RC, Eagles PM, Ng BS. The effect of radius ratio on the stability of Couette flow and Taylor vortex flow. Physics of Fluids. 1984;**27**(10):2403-2411

[35] Desmet G, Verelst H, Baron GV. Local and global dispersion effects in Couette-Taylor flow—I. Description and modeling of the dispersion effects. Chemical Engineering Science. 1996; **51**(8):1287-1298

[36] Takeda Y. Quasi-periodic state and transition to turbulence in a rotating Couette system. Journal of Fluid Mechanics. 1999;**389**:81-99

[37] Haut B, Amor HB, Coulon L, Jacquet A, Halloin V. Hydrodynamics and mass

transfer in a Couette–Taylor bioreactor for the culture of animal cells. Chemical Engineering Science. 2003;**58**(3–6): 777-784

[38] Soos M, Wu H, Morbidelli M. Taylor-Couette unit with a lobed inner cylinder cross section. AICHE Journal. 2007;**53**(5):1109-1120

[39] Atsumi K, Makino T, Kato K, Murase T, Iritani E, Chidphong P, et al. Frictional resistance of grooved rotor in cylindrical dynamic filter chamber without permeation or throughflow. Kagaku Kogaku Ronbunshu. 1988;**14**(1): 14-19

[40] Lewis GS, Swinney HL. Velocity structure functions, scaling, and transitions in high-Reynolds-number Couette-Taylor flow. Physical Review E. 1999;**59**(5):5457

[41] Mao KW, Toor HL. A diffusion model for reactions with turbulent mixing. AICHE Journal. 1970;**16**(1): 49-52

[42] Ottino JM, Ranz WE, Macosko CW. A lamellar model for analysis of liquid-liquid mixing. Chemical Engineering Science. 1979;**34**(6):877-890

[43] Fournier MC, Falk L, Villermaux J. A new parallel competing reaction system for assessing micromixing efficiency—experimental approach. Chemical Engineering Science. 1996; **51**(22):5053-5064

[44] Baldyga J, Bourne JR. Principles of micromixing. Encyclopedia of fluid mechanics. Vol. 11986. Houston, TX: Gulf Publishing Co. pp. 147-201

[45] Brunsteiner M, Jones AG, Pratola F, Price SL, Simons SJ. Toward a molecular understanding of crystal agglomeration. Crystal Growth & Design. 2005;**5**(1): 3-16

[46] Dehkordi AM, Vafaeimanesh A. Synthesis of barium sulfate nanoparticles using a spinning disk reactor: Effects of supersaturation, disk rotation speed, free ion ratio, and disk diameter. Industrial & Engineering Chemistry Research. 2009;**48**(16): 7574-7580

[47] Crowe CT, Troutt TR, Chung JN. Numerical models for two-phase turbulent flows. Annual Review of Fluid Mechanics. 1996;**28**(1):11-43

[48] Haider A, Levenspiel O. Drag coefficient and terminal velocity of spherical and nonspherical particles. Powder Technology. 1989;**58**(1):63-70